(2)

SAR-Related Stress Variability in the Marine Atmospheric Boundary Layer (MABL)
(High-Resolution ARI)

Hampton N. Shirer and George S. Young
Penn State University
Department of Meteorology
503 Walker Bldg
University Park, PA 16802
(814) 863-1992 (HNS)
(814) 863-4228 (GSY)
(814) 865-3663 (FAX)
HNS@PSUVM.PSU.EDU (HNS)
G.YOUNG/OMNET (GSY)
YOUNG@EMS.PSU.EDU (GSY)

PROJECT ABSTRACT

By stressing the sea surface, the marine atmospheric boundary layer (MABL) can alter the sea surface wave field and so can produce discernible signatures on SAR images of the ocean (e.g. Visecky and Stewart 1982). Among the resulting signatures, the quasi-linear and cellular microscale patterns still require adequate explanation. The ubiquitous MABL two- and three-dimensional convective circulations provide promising candidates for the forcing phenomena producing these signatures. These microscale circulations have horizontal wavelengths on the order of one to ten times the boundary layer depth, or approximately one to ten km, and temporal scales on the order of one to ten hours. Thus, they produce stress variations on the spatial and temporal scales of the quasi-linear and cellular SAR signatures.

Long Term Goals:

Our ultimate goal is to develop methods for diagnosing both the form and the effect on sea-surface stress patterns of buoyantly-forced MABL flows given only values of the large-scale meteorological and oceanographic parameters. As briefly summarized below, we continue to make strong progress on this problem using several interacting, complementary techniques that range from data analysis to model development.

Near Term Objectives:

Our most immediate goal is to determine how effective the two-and three-dimensional buoyantly forced MABL circulations with scales on the order of 0.1 to 10 km are in producing microscale patterns of sea-surface stress variability that can be directly linked to the quasi-linear and cellular SAR signatures that were observed during the Hi-Resolution ARI experiment and by earlier, satellite

mounted, sensors. Two primary objectives must be met for us to achieve these goals. First, the surface layer structure within the MABL must be related to the sea-surface stress patterns for the solenoidal MABL circulation associated with quasi-linear sea-surface temperature (SST) gradients and for each of the three microscale atmospheric boundary layer convective forms: the two-dimensional mixed-layer rolls, the three-dimensional mixed-layer thermals, and the surface layer plumes. Second, the environmental conditions necessary and sufficient for the formation of each of these buoyantly-driven circulations must be identified.

Approach:

The convective component of the first objective has been completed as the MS thesis of Todd Sikora (Sikora 1992; Sikora and Young, 1993) by using both conditional sampling and composite analysis of atmospheric surface layer observations to describe the occurrence, structure, and sea-surface stress and wind patterns of MABL convection. Aircraft data from the marine stratocumulus-topped boundary layers observed during Project FIRE [First ISSCP (International Satellite Cloud Climatology Program) Regional Experiment] were used for the data analysis. Conditional sampling of these boundary-layer data identified updrafts and downdrafts, while composite analysis was used to summarize the spatial (planview) variations within updrafts and downdrafts to quantify the average structure of each. Current work focuses on preparation of a technical memorandum detailing how to use these results as forcing in ocean wave models. This task will be followed by a comparison of these observational results with output from the new, intermediate-order models described below.

With the observational analysis of microscale convection nearing completion, we are proceeding to the next MABL phenomenon of interest to the Hi-Resolution ARI community, the MABL solenoidal circulation associated with the sharp SST gradient along the northwest wall of the Gulf Stream. Observations from the two ARI cruises will be used to create similar composite analyses of this somewhat larger scale, yet still buoyantly driven, flow. The ship-based sensors deployed during both cruises by Penn State and collaborators from Wood's Hole Oceanographic Institute will permit measurements of this MABL response to the ocean front as well as the resulting feedback to the wave field via cross-front variations in the wind and stress. Cross-front sampling legs and along-front legs with two ships paired across the front will yield maximum information on the role of the SST gradient in forcing the observed horizontal variations of the surface wave field.

Elucidation of the stress variability expected in different forcing regimes is being achieved by the development and study of new two-dimensional and three-dimensional intermediate-order spectral models of MABL convection. The first, a lower resolution version following the boundary layer roll model of Haack and Shirer (1992), is the MS thesis project of Peter Bromfield. The second is a higher resolution three-dimensional convective model whose development was

begun by Julie Schramm and will be continued by MS student Louis Zuccarello. In both these models, the boundary conditions are based on boundary layer similarity theory and so are sufficiently general that the surface stress can be nonzero.

To help guide comparison of observed and modeled results, algorithms for adequately estimating such chaos measures as the correlation dimension are needed as well as a means for estimating the probable errors in these estimates. We have developed such an algorithm (Wells *et al.* 1993), and MS student Christian Fosmire has applied this algorithm to boundary layer wind data.

Recent Tasks Completed:

The conditional sampling and composite analysis of the planview patterns of surface stress variability caused by MABL convective updrafts and downdrafts has been completed with the results accepted for publication (Sikora 1992; Sikora and Young 1993) and presented at the Tenth Symposium on Turbulence and Diffusion (Sikora and Young 1992).

Meteorological observations and infrared satellite images have been acquired for interpretation of an ERS-1 SAR feature in collaboration with Hi-Resolution ARI researcher Robert Beal of Johns Hopkins University's Applied Physics Laboratory (APL).

In collaboration with Don Thompson, another ARI researcher at APL, data acquisition and theoretical explanation have been completed for the MABL front and solenoidal circulation observed during a transect of the Gulf Stream ocean front by the RV Vernadsky. Mesoscale atmospheric simulations of the similar flows observed during the first Hi-Resolution ARI cruise in Fall 1991 were completed in real time using the Penn State mesoscale model MM4, which was also used to provide daily forecast support to the cruise planners.

A version of the three-dimensional intermediate-order model was integrated and preliminary results showed that the forms of the stress and heat flux profiles were correct and matched those observed in the stratocumulus-topped MABL by Brümmer and Busack (1990). The energy budget properties were not completely correct, however, and appear to be caused in part by an improper handling of the pressure gradient term in the equation of motion. Because this term is much easier to handle in a two-dimensional model, we undertook the development of such a model as the MS thesis project for Peter Bromfield. We also began a reexamination of the formulation of the three-dimensional model; the corrected formulation will be implemented by MS student Louis Zuccarello.

The correlation dimension algorithm of Wells *et al.* (1993) was supplemented with means for estimating the relative error in the estimate of this

dimension. Christian Fosmire applied this algorithm to boundary layer wind data and determined that, when an estimate of the relative error is included, the dimension values given by either horizontal wind component are the same as those expected from theory; without considering these error estimates, the dimension values would appear to be different (Fosmire 1993).

Results:

The published analyses of the composite structure of MABL updrafts and downdrafts (Sikora 1992; Sikora and Young 1992, 1993) provide the first-ever quantitative description of the planview patterns of air/sea fluxes of momentum, heat, and moisture. Figure 1 shows the corresponding composite planview perturbation wind field for MABL convective downdrafts, the phenomenon that drives "cat's paw" wave patterns on the sea surface. These results can be used by ocean-wave modelers to quantify the horizontal variability of atmospheric forcing on spatial scales on the order of 0.1 to 1.0 km.

Preliminary theoretical analysis suggests that a solenoidal circulation, akin to the classic sea-breeze circulation, causes the significant MABL wind variations observed in the vicinity of the northwest wall of the Gulf Stream. This common phenomenon is revealed by a cloud line in meteorological satellite and Hi-Resolution cruise observations as well as by the band of altered wind direction in the MM4 mesoscale model forecasts and the RV Vernadsky transect. Further analysis of observations from the second Hi-Resolution ARI cruise and quantitative diagnostics of the MM4 results will be required to complete the description of this phenomenon, its effect on the sea-surface stress field, and the range of conditions under which it can occur.

A manuscript, Wells *et al.* (1993), summarizing the new algorithm for estimating the correlation dimension and its probable error is nearly completed and will be submitted to *Physica D* in 1993. A preliminary description of the results in this paper was presented at the Spring 1992 AGU conference in Montreal, Canada (Wells *et al.* 1992). This algorithm has been applied to boundary layer wind observations by Fosmire (1993) and is ready to be applied to other modeled and observed MABL datasets.

Accomplishments:

A graduate student (Todd Sikora) has completed his MS thesis (Sikora, 1992) on the patterns of horizontal variability in sea-surface forcing caused by MABL convection. These results have been presented by George Young at the April 14-16, 1992 Hi-Resolution Workshop at APL, by Todd Sikora at the Tenth Symposium on Turbulence and Diffusion in Portland, Oregon, September 29-October 2, 1992 (Sikora and Young 1992), and have been accepted for publication in *Boundary-Layer Meteorology* (Sikora and Young 1993). Todd Sikora and George Young have also pursued a meteorological explanation for an

ERS-1 SAR feature noted by Robert Beal. A new graduate student (Sean Sublette) is being taught to analyze mesoscale model output in conjunction with Hi-Resolution cruise observations to develop a composite description of the flow and stress fields associated with the MABL solenoidal circulation that is forced by the Gulf Stream ocean front. Theoretical insight into this frequently occurring phenomenon has been provided to interested ARI investigators, Don Thompson and Farid Askari. Also, George Young helped plan the next Hi-Resolution cruise at the October 27-29, 1992 workshop at NRL. Graduate students Peter Bromfield and Louis Zuccarello are developing two- and three-dimensional models of the stress variability caused by MABL circulations; these models are extensions of the first version coded by research associate Julie Schramm. Preliminary results from this version were presented by Nels Shirer at the April 14-16, 1992 Hi-Resolution Workshop. Finally, MS student Christian Fosmire has applied the Wells *et al.* (1993) algorithm to boundary layer wind data; he is writing his thesis (Fosmire 1993) for an expected May 1993 graduation. This algorithm was also presented by Christian Fosmire at the Spring 1992 AGU meeting in Montreal, Canada (Wells *et al.* 1992).

References:

Brümmer, B. and B. Busack, 1990: Convective patterns within a field of stratocumulus. *Mon. Wea. Rev.*, **118**, 801-817.

Fosmire, C.J., 1993: Estimating the correlation dimension of observed boundary layer winds. MS Thesis, Penn State University, in preparation.

Haack, T. and H.N. Shirer, 1992: Mixed convective/dynamic roll vortices and their effects on initial wind and temperature profiles. *J. Atmos. Sci.*, **49**, 1181-1201.

Sikora, T.D., 1992: Air/sea flux patterns within convective structures of the marine atmospheric surface layer, MS Thesis, Penn State University, 28 pp.

Sikora, T.D and G.S. Young, 1992: Air/sea flux patterns within convective structures of the marine atmospheric surface layer, Preprints, *Tenth Symposium on Turbulence and Diffusion*, Sept. 29-Oct. 2, 1992, Portland, OR, American Meteorological Society, 25-27.

Sikora, T.D. and G.S. Young, 1993: Observations of planview flux patterns within convective structures of the marine atmospheric surface layer, *Boundary Layer Meteorology*, **35**, in press.

Visecky, J.F. and R.H. Stewart, 1982: Observation of ocean surface phenomena using imagery from the SEASAT synthetic aperture radar. *J. Geophys. Res.*, **87**, 3397-3430.

Wells, R., H.N. Shirer and C.J. Fosmire, 1992: An improved algorithm for calculating the correlation dimension and for estimating its probable error, AGU Spring 1992 Conference, May 12-16, 1992, Montreal, Canada, American Geophysical Union.

Wells, R., H.N. Shirer, C.J. Fosmire and J. Doran, 1993: Improved algorithms for estimating the correlation dimension and the associated probable errors. To be submitted to *Physica D*.

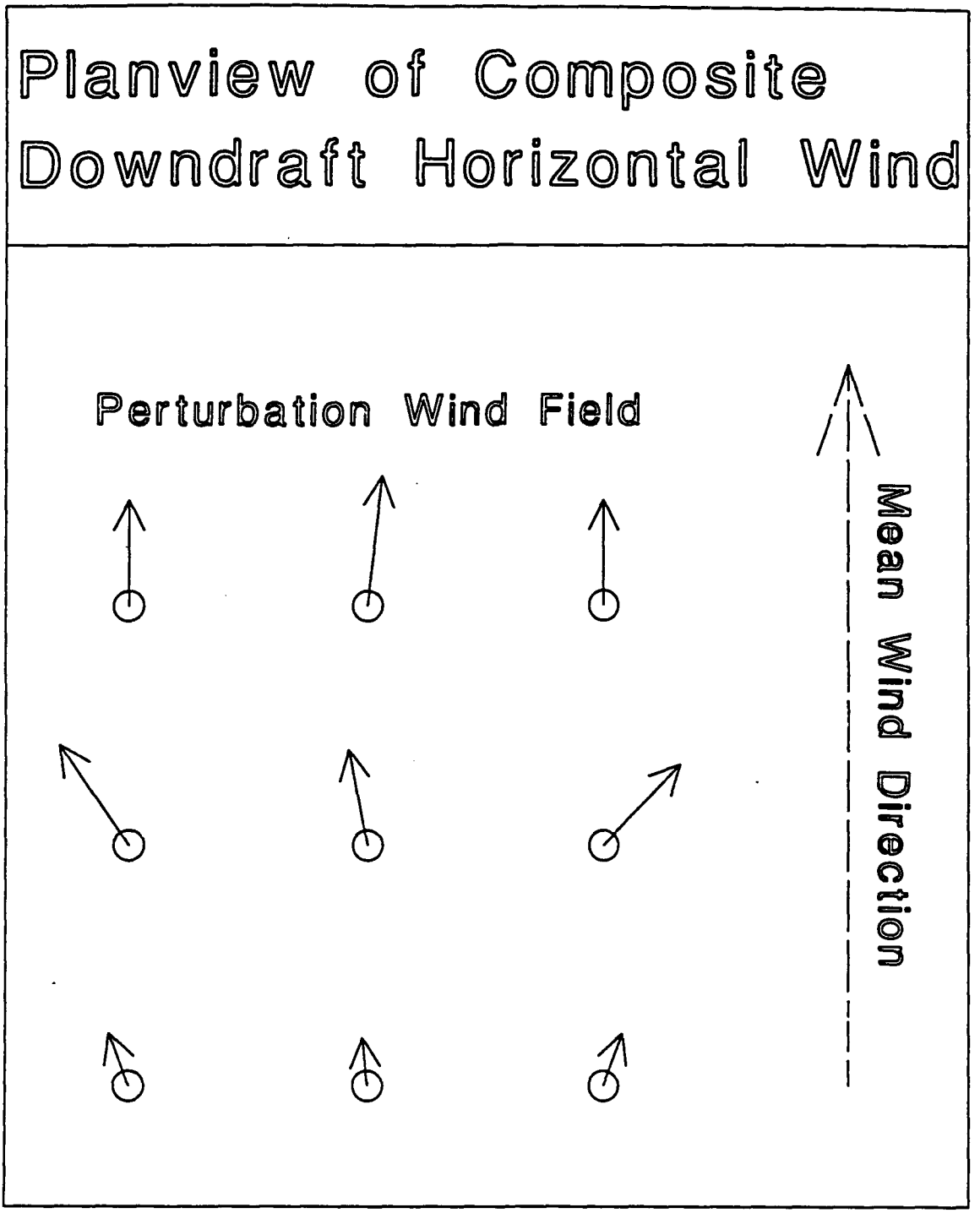

Figure 1 Planview of composite horizontal wind in MABL convective downdrafts in the surface layer.

PUBLICATIONS/PRESENTATIONS/REPORTS—FY91/FY92
HAMPTON N. SHIRER AND GEORGE S. YOUNG, PI
DECEMBER 1992

92-R Fosmire, C.J., Estimating the correlation dimension of observed boundary layer winds. MS Thesis, Penn State University, in preparation (1993).

92-R Hare, J.E, Shipboard eddy-covariance measurements of the turbulent fluxes of heat, moisture, and momentum. MS Thesis, Penn State University, 207 pp. (1992).

92-R Sikora, T.D., Air/sea flux patterns within convective structures of the marine atmospheric surface layer, MS Thesis, Penn State University, 28 pp. (1992).

92-C, 92-R Sikora, T.D and G.S. Young, Air/sea flux patterns within convective structures of the marine atmospheric surface layer, Preprints, *Tenth Symposium on Turbulence and Diffusion*, Sept. 29-Oct. 2, 1992, Portland, OR, American Meteorological Society, 25-27 (1992).

92-PS Sikora, T.D. and G.S. Young, Observations of planview flux patterns within convective structures of the marine atmospheric surface layer, *Boundary Layer Meteorology*, **35**, in press (1993).

92-PI Sikora, T.D. and G.S. Young, Methods for use planview flux patterns in air/sea interaction applications, Technical memorandum in preparation, Penn State University (1993).

91-R, 91-C Thomson, D.W., H.W. Henderson, and C.J Fosmire, Using remote sensing systems to estimate attractors for meteorological variables. Preprints, *Second Symposium on Tropospheric Profiling: Needs and Technologies*, Boulder, CO, Sept. 10-13, 1991 (1991).

91-IC Thomson, D.W. and H.W. Henderson, Attractor-based interpretation of measurements made with radar and acoustic remote sensing systems. *EPP-Fall 1991 Symposium on Remote Sensing of the Propagation Environment*, Sept. 30-Oct. 4, 1991, Cesme-Ismir, Turkey (1991).

91-IC, 92-R Thomson, D.W. and H.W. Henderson, Definition of local atmospheric attractors using measurements made with surface-based remote sensing systems. *Proc. of the First Experimental Chaos Conference*, Oct. 1-3, 1991, Arlington, VA. World Scientific Publishing Co., 389-402 (1992).

PUBLICATIONS/PRESENTATIONS/REPORTS—FY91/FY92 (CONT)
HAMPTON N. SHIRER AND GEORGE S. YOUNG, PI
DECEMBER 1992

92-C Wells, R., H.N. Shirer and C.J. Fosmire, An improved algorithm for calculating the correlation dimension and for estimating its probable error, AGU Spring 1992 Conference, May 12-16, 1992, Montreal, Canada, American Geophysical Union (1992).

92-PI Wells, R., H.N. Shirer, C.J. Fosmire and J. Doran, Improved algorithms for estimating the correlation dimension and the associated probable errors. *Physica D*, in preparation (1993).

OBSERVATIONS OF PLANVIEW FLUX PATTERNS WITHIN CONVECTIVE STRUCTURES OF THE MARINE ATMOSPHERIC SURFACE LAYER

Todd D. Sikora and George S. Young

The Pennsylvania State University

August 1992

To appear in Boundary Layer Meteorology

Table of Contents

List of Figures

List of Tables

Abstract. Air/sea flux variability on horizontal scales from 50 m to several km results, in part, from the presence of coherent convective structures within the atmospheric boundary layer. The horizontal distribution of fluxes within these convective updrafts and downdrafts is, therefore, central to studies of air/sea interaction and remote sensing of sea surface wind and wave fields. This study derives these flux patterns from observations of the Marine Atmospheric Surface Layer (MASL).

Research aircraft flights through the MASL provide an optimal means for sampling large numbers of the above-mentioned coherent structures. The NCAR Electra flew numerous legs through the MASL at a height of 50 m during the 1987 stratocumulus phase of Project FIRE (First ISSCP (International Satellite Cloud Climatology Program) Regional Experiment). In situ measurements from these legs serve as the dataset for this paper. The data are processed in such a way as to retain only the turbulence fluctuations. Conditional sampling, based on the vertical velocity field, results in the isolation of convective updrafts and downdrafts. Compositing of the data for these two classes of convective drafts results in horizontal planviews of the vertical fluxes of buoyancy, absolute humidity, along-mean-wind component of momentum, and vertical velocity. To ensure dynamical similarity, these horizontal planviews are oriented in a coordinate system aligned with the mean wind.

1. Introduction

The marine atmospheric surface layer (MASL) ($Z \leq 0.1\ Z_i$ where Z_i is the boundary layer depth) (Stull, 1989) plays a major role in air/sea interaction. It is the MASL that couples the sea surface to the overlying atmospheric boundary layer through vertical eddy fluxes (hereafter referred to simply as fluxes), such as those of buoyancy, moisture, and momentum. While these fluxes are present in both stable and unstable environments, they tend to be enhanced by convective elements, as is implied by bulk aerodynamic parameterization (e.g. Liu et al., 1979). For this reason, much of the recent research in this area has concentrated on the convective marine atmospheric surface layer (CMASL).

CMASL fluxes are realized through sub-mesoscale convective updrafts (CUs) and downdrafts (CDs). These features have diameters on the order of tens to thousands of meters (Lenschow and Stephens, 1980). Khalsa and Greenhut (1985) found that within a central Pacific CMASL, such features were responsible for 75% of the total flux of heat, moisture, and momentum. This importance provides the motivation to explore further the flux characteristics of CMASL drafts.

Various methods may be employed to study CMASL drafts. Qualitatively, this can be accomplished by simply observing the effects their associated fluxes have on the environment.

On a human scale, anyone who has enjoyed a day of sailing, seen wisps of sea fog, or witnessed cats paws rippling across a body of water has personally sensed the impact of CMASL drafts on the environment. Another example of this manifestation can be seen in Figures 1 and 2. Figure 1 is

Photos are not available at this time.

Fig. 1. Visible image from the Kosmos 1500 satellite.

Fig. 2. X-band real aperture radar image of the underlying sea surface.

a visible image from the Kosmos 1500 (Okean) satellite. The image is centered at 26° N 125.5° W and is dated July 11, 1984. It shows common boundary layer cumuliform clouds, horizontal scales of which are on order of the boundary layer depth, induced by fluxes of heat and moisture within CMASL-born CUs. Figure 2 is the corresponding X-band real aperture radar image of the underlying sea surface. It depicts a perturbed sea surface wave pattern resulting from CMASL momentum flux patterns driven by flow into CUs and out of CDs.

In order to obtain data on the effects and structure of CUs and CDs in a more quantitative sense, various techniques have been employed, including observations from a sensor

equipped catamaran (Dorman and Mollo-Christensen, 1973), the use of acoustic sounders (Gaynor and Mandics, 1978), and observations of sea gulls in flight (Woodcock, 1940, 1975). Data for the quantitative study in this paper are obtained from NCAR Electra aircraft flights during the First ISCCP (International Satellite Cloud Climatology Project) Regional Experiment (FIRE). Flights were conducted over a several hundred kilometer region west of the southern California coast during June and July, 1987. For detailed reviews of the FIRE project, see Albrecht et al. (1988) and Kloesel et al. (1988).

The traditional way to investigate the flux characteristics of boundary layer features is through conditional sampling and composite analysis, examples of which are discussed below. Simply put, conditional sampling uses an indicator function to isolate from a dataset features of interest (e.g. CUs and CDs). Composite analysis then combines information from these selected features to determine their average spatial structure.

In the past, various studies have gathered valuable information concerning boundary layer features using these sampling and analysis techniques. Wilczak and Tillman (1980) and Wilczak (1984) used Boulder Atmospheric Observatory tower data to produce detailed, land-based, statistics for convective atmospheric surface layer features known as temperature ramps. Young (1988) also investigated land-based turbulence at the Boulder Atmospheric Observatory. He

conditionally sampled aircraft data, based upon vertical velocity perturbations and mixed layer spectra of vertical velocity and temperature, in order to analyze thermals within the convective boundary layer. Lenschow and Stephens (1980) used NCAR Electra aircraft data to generate information on the structure of marine atmospheric boundary layer (MABL) thermals using humidity as an indicator function. Greenhut and Khalsa (1982) and Khalsa and Greenhut (1985) also used aircraft data to study properties of drafts in the MABL but, as in Young (1988), they used vertical velocity as an indicator of a feature. In addition to observational studies, large-eddy simulation models, such as that of Schumann and Moeng (1991), have been used to provide boundary layer datasets for conditional sampling and compositing.

While previous work has resulted in detailed vertical profiles of properties of MABL updrafts and downdrafts, information on planview flux variability of CMASL CUs and CDs is lacking. To fill this need, this study utilizes conditionally sampled and composited eddy correlated FIRE aircraft data to investigate the typical CMASL CU and CD planview patterns of vertical velocity flux, $w'w'$, buoyancy flux, $w'T_v'$, absolute humidity flux, $w'r'$, and along-mean-wind momentum flux, $w'u'$. Note that while CUs and CDs are segregated in this study, the techniques used for their analyses are identical.

2. Procedures

The use of NCAR Electra turbulence data from project FIRE is advantageous for the type of research discussed here because a properly instrumented aircraft provides a means for collecting high resolution turbulence data from a large number of CMASL drafts. While each draft can be penetrated only once, penetrations of many different drafts can be made from numerous angles. In addition, the turbulence data from a draft sampled by an aircraft can be looked upon as a snapshot of that feature (see sub-section 2.3.). The result, after data processing, conditional sampling, and compositing, is a statistically robust planview flux description of a typical CMASL draft.

2.1. FLIGHT INFORMATION

Of the numerous available datasets collected from Electra flight legs during FIRE, only the 20 used in this study were conducted within the CMASL. These legs averaged 50 km (500 sec) in length (duration). These legs were flown on seven different days, during which the average boundary layer depth was 920 m. The legs were flown at a height of 50 m, well within the depth of the surface layer. The ratio of the boundary layer depths to the Monin-Obukhov lengths ranged from -0.62 to -37.56, indicative of slightly to moderately unstable

MABLs. While flux intensity differences for CUs and CDs are seen within this stability range, the "flux-shapes" (the patterns of spatial variation of flux magnitude across a draft) are similar. This pattern similarity in the presence of intensity differences is exactly analogous the geometric similarity of "similar triangles" of varying sizes. Structural differences are, however, observed for stable and extremely unstable cases. Insufficient data prevented the extension of the composite analysis to these other stability ranges.

2.2. INSTRUMENTATION AND DATA PROCESSING

The Electra CMASL 20 hz turbulence data used in the present study include vertical velocity, w, air temperature, T, absolute humidity, r, and the aircraft-oriented components of the wind, u, and, v. This sampling rate combined with the 100 m/s aircraft speed yields a minimum resolvable wavelength of 10 m. A review of the aircraft instrumentation of significance to this study can be found in Nucciarone and Young (1991). Data processing for mean, trend, and spike removal, as well the derivation of buoyancy flux, parallels that of Moyer and Young (1991). In order to eliminate contributions by mesoscale phenomena in the data, high-pass filtering is employed following the techniques of Young (1987,1988).

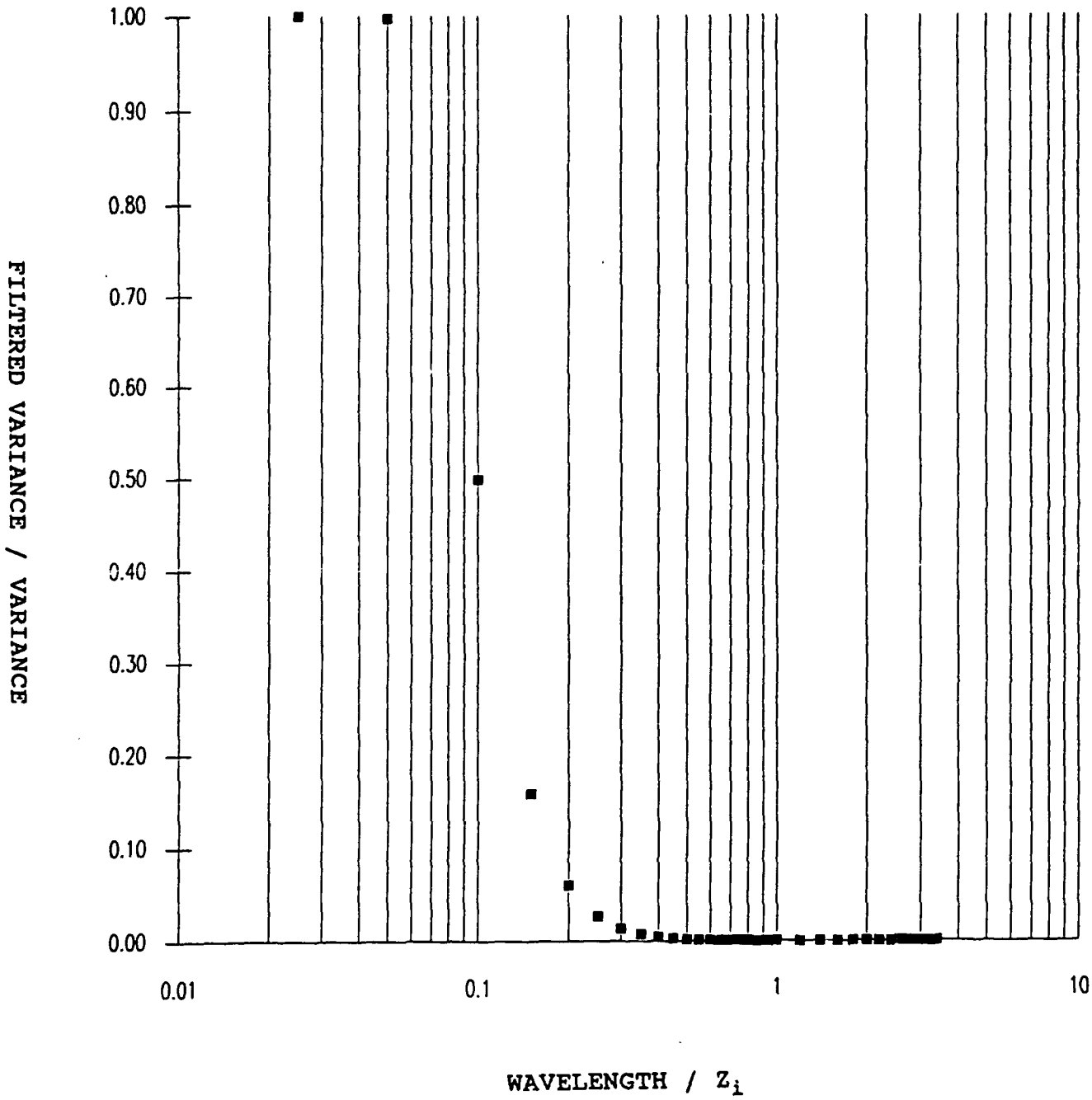
1.00
0.90
0.80
0.70
0.60
0.50
0.40
0.30
0.20
0.10
0.00
0.01
0.1
1
10
FILTERED VARIANCE / VARIANCE
WAVELENGTH / z_i

Figure 3

An example of the spectral response of the filter can be seen in Figure 3. The figure shows, for a cosine wave, how

Fig. 3. An example of the spectral response of the filter.

the ratio of the wave's filtered variance to its unfiltered variance varies with the ratio of wavelength to Z_i. In this example, the cutoff wavelength chosen is 0.1 Z_i. At this wavelength, 50% of the wave's original variance remains. At longer wavelengths, the amount of the wave's original variance remaining after filtering diminishes rapidly.

FIRE spectra of Nucciarone and Young (1991) indicate that 1.5 Z_i is the appropriate mesoscale subrange cutoff wavelength for use in the filter. The net result of this data processing, for any one variable, is a sub-mesoscale

perturbation series (denoted by primed variables) suitable for computing eddy correlation statistics.

Coordinate rotations are performed on the perturbation wind components yielding one component in the direction of the mean wind, u', and another aligned with positive values 90° to the left of the mean wind, v'. Unlike that seen in Geernaert and Hansan (1992), where orographic distortion of the low level flow may be occurring, the cross-mean-wind components of the momentum fluxes of this study are both statistically and physically insignificant when compared with the along-mean-wind component (i.e. mean < standard deviation for $w'v'$ and $w'v' << w'u'$). For this reason, the cross-mean-wind momentum flux will not be discussed.

2.3. CONDITIONAL SAMPLING

In order to distinguish updrafts and downdrafts, event criteria based on perturbation vertical velocity are required. Greenhut and Khalsa (1982) and Young (1988) show that w' event criteria, incorporating germane horizontal scales and magnitude thresholds, allow for the proper detection of boundary layer features of interest.

In order to distinguish CUs and CDs, the w' series is first band-pass filtered to retain only the convective scales (Young 1988). The band-pass filter is a variation on that discussed in sub-section 2.2., combining both a high-pass and

low-pass stage. It is designed to eliminate both the mesoscale and inertial subrange contributions to the w′ series, while still preserving the CUs and CDs of the energy containing subrange. As discussed in sub-section 2.2., 1.5 Z_i is used as the mesoscale subrange cutoff wavelength. The choice of an inertial subrange cutoff wavelength is 0.1 Z_i. As in Young (1988), this choice eliminates scales of motion associated with the inertial cascade.

Given the average Z_i of this study, a minimum draft width of 50 m is chosen so that the narrowest acceptable event (CU/CD couplet) corresponds with the 0.1 Z_i inertial subrange cutoff wavelength used in the band-pass filter. All drafts not meeting the minimum width criteria are rejected because of their inertial subrange character.

The literature mentioned in section 1. provides numerous examples of conditional sampling magnitude thresholds designed to distinguish features of interest from their environment. Inspection of the FIRE w′ data series suggests that a w′ threshold of ± 0.1 m/s eliminates disorganized areas of weak ascent or decent. Any data points for which $w' < 0.1$ m/s are therefore considered not to be part of significant convective features and are so rejected.

CUs (CDs) are then defined to be features within the band-pass filtered w′ data series meeting these minimum width and magnitude criteria. The total number of CUs sampled and used in compositing is 2839, averaging 98 m in width and

occupying 28% of the data series. The total number of CDs sampled and used in compositing is 3062, averaging 107 m in width and occupying 33% of the data series. Given the above widths and an aircraft velocity of 100 m/s, it can be shown that Taylor's Hypothesis is valid (Stull 1989). Draft composites of eddy correlation statistics can therefore be looked upon as typical planview flux snapshots of a CU or a CD.

2.4. COMPOSITING OF EDDY CORRELATION STATISTICS

After the isolation of CUs and CDs, eddy correlation fluxes of vertical velocity, buoyancy, absolute humidity, and along-mean-wind momentum are calculated from the high-pass filtered dataset, for each draft. Note that, unlike the band-passed series used to locate the sub-mesoscale CUs and CDs, this series retains the inertial subrange contributions. Only the mesoscale contributions are filtered out, as discussed in sub-section 2.2.. In order to develop typical planview flux snapshots, the fluxes from all the drafts are composited together using the series of averaging calculations and grouping techniques discussed below.

Each draft is first divided into 3 bins of equal length: the aircraft entry region of the draft, bin (a), the middle of the draft, bin (b), and the aircraft exit region of the draft, bin (c). The average CU and CD flux patterns for each leg are

then found by calculating bin average eddy correlation statistics as follows. The flux of any variable y by variable w′ is found by first taking the sum of their product over all points of all like bins [bin (a), (b), or (c)] over all like drafts (CUs or CDs) within the leg. This sum is then divided by the number of data points in all like bins of all like drafts within the leg.

The resulting 40 leg average drafts (LADs) from the 20 flight legs are then separated into one of 3 equal angular-width groups. The grouping of an LAD depends on the path taken by the aircraft, through the draft, relative to the mean wind. In polar coordinates with the mean wind vector aligned towards 0°, these relative heading groups are: along-mean-wind (330° to 30° and 150° to 210°), cross-mean-wind (60° to 120° and 240° to 300°), and diagonal-to-the-mean-wind (the remaining relative heading ranges).

To maintain wind-relative consistency in bin naming, flux data for bins (a) and (c) are switched for those drafts of the along-mean-wind and diagonal groups whose relative headings oppose the mean wind. The same is done for LADs of the cross-mean-wind group whose relative heading range is aligned to the left of the mean wind. Note that while there are twice as many relative heading ranges for the diagonal group as for the other two, the angular width of each heading range in the diagonal group is only half as large as for the other two. Thus, the angular coverage of all 3 groups is equal.

The two remaining relative-heading ranges of the diagonal group (30° to 60° and 300° to 330°) can be merged using symmetry arguments. Wilczak (1984) shows mirror symmetry of the horizontal perturbation wind field about an axis aligned with the mean wind extending through the center of his large-scale eddy (LSE which is a CU/CD couplet). A similar symmetry can be seen in the current dataset by examination of the fluxes of the cross-mean-wind group composites found in section 3.. Comparison of the data from the two relative heading ranges of the diagonal group (not shown) demonstrates symmetry across the axis of the mean wind for both the upwind and downwind ends of the drafts. Taking these symmetries into account, flux data of like LAD downwind bins of the diagonal group are composited together as are flux data of upwind bins. Figure 3 shows the spatial relation of the three groups within a planview draft. Bins are labeled (a), (b), or (c). Upper case letters indicate the group to which each bin belongs; the along-mean-wind group (A), the cross-mean-wind group (C), and the diagonal-to-the-mean-wind group (D). The mean wind vector is assumed to be directed towards the top of the figure.

The process of compositing flux data of like LAD bins into a flux for the corresponding bins of a group average draft (GAD) will now be explained. First, because the center bin for all groups corresponds to the same part of the draft, the average bin (b) flux over all like LADs over all groups

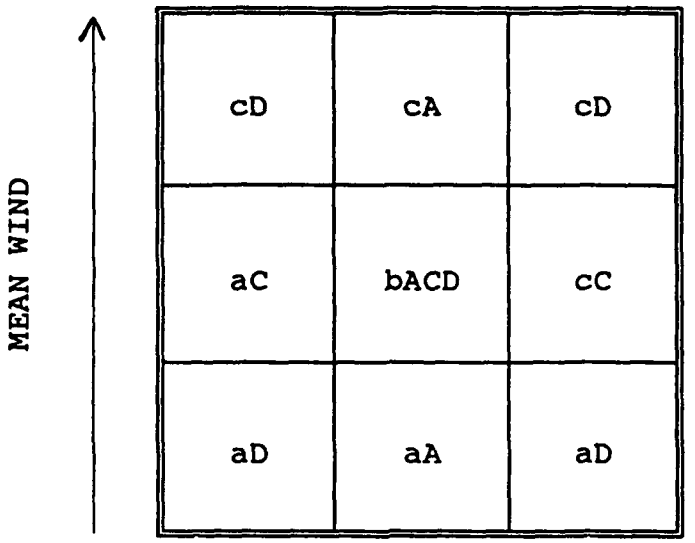

Fig. 4. The spatial relation of the three groups within a planview draft.

(bin (b) average) may be used to represent the flux in the center bin of all groups. As stated in sub-section 2.1., drafts of each leg are structurally similar in terms of their flux-shape. However, there is a need to correct for mean draft intensity differences between like bins of different LADs. It follows then that LAD bin (a) and (c) fluxes are rescaled before any averaging to produce GADs. This rescaling uses a correction coefficient based on the need for inter-leg similarity in bin (b), described above. This correction coefficient is bin (b) average divided by the respective LAD bin (b). This approach is robust because the LAD bin (b) fluxes of all the quantities studied are generally large and of same sign.

The final planview composite is found by simply overlaying the along-mean-wind, cross-mean-wind, and diagonal-

to-the-mean wind (again using symmetry for the second diagonal) GADs for each statistic discussed.

3. Observational Results

Planview draft flux composites of vertical velocity, buoyancy, absolute humidity, and the along-mean-wind component of momentum, along with corresponding bin standard deviations, are presented in Tables I through VIII. Each table is a three by three array of group bin fluxes. Bin location in this array corresponds to its position within the composite draft. In all tables, the mean wind is directed towards the top of the table. For each composite, then, the along-mean-wind group axis is aligned from the upwind center to downwind center, the cross-mean-wind group axis is aligned from the middle left to middle right, and the diagonal group makes up the remainder.

Note that the middle center bin of all tables is its respective bin (b) average of sub-section 2.4.. Recall also that the middle center bin is used to rescale all other bins within a flux composite. For these reasons, the majority of the uncertainty associated with any flux-shape and intensity related interleg differences, associated with interleg differences in the middle center bins, is forced into the perimeter of the composite array. It follows then that standard deviations for the middle center bins are not given.

3.1. VERTICAL VELOCITY FLUX

Vertical velocity dictates, to a large extent, the other flux patterns discussed in this study. Not only is it used for the defining of events, but also it is the flux variable doing the work, so to speak, by advecting the other quantities. The planview CU w'w' composite is presented in Table I.

TABLE I

CU vertical velocity flux composite and corresponding standard deviations.

$w'w'(m^2s^{-2})$ (std. dev.)	Left	Center	Right
Downwind	0.227 (0.015)	0.244 (0.040)	0.227 (0.015)
Middle	0.217 (0.023)	0.341	0.225 (0.021)
Upwind	0.238 (0.009)	0.266 (0.016)	0.238 (0.009)

Because all bin standard deviations are much smaller than the bin fluxes, there is statistical confidence in the entire CU w'w' composite. The strongest flux region is found along the along-mean-wind group axis with the largest magnitude of

flux being at the center of the composite. This shape compares well with that found at 50 m over land by Wilczak (1984). Examining the perimeter of the composite, the flux magnitude along the upwind side of the draft tends to be larger than that along the downwind side, although these asymmetries are less statistically significant than the radial variation. The weakest flux is found in the middle right and left bins.

The planview CD vertical velocity flux composite is shown in Table II. As with the CU composite, there is

TABLE II

CD vertical velocity flux composite and corresponding standard deviations.

$w'w'(m^2s^{-2})$ (std. dev.)	Left	Center	Right
Downwind	0.160 (0.011)	0.161 (0.018)	0.160 (0.011)
Middle	0.171 (0.024)	0.204	0.173 (0.024)
Upwind	0.162 (0.009)	0.166 (0.019)	0.162 (0.009)

statistical confidence in all bin fluxes. While the largest magnitude of w'w' is again found in the center middle bin, the over all flux composite is weaker than that of the CU. This finding is in agreement with those of Greenhut and Khalsa (1982) for their coherent downdrafts. As with the CU composite, other aspects of the w'w' pattern are less statistically significant. The strongest flux region is found along the cross-mean-wind group axis. Flux along the upwind side of the draft is slightly larger than that along the downwind side.

3.2. BUOYANCY FLUX

The buoyancy flux of the current study has the same sign and approximates to a large extent the magnitude of the heat-flux w'T'. The planview CU buoyancy flux composite is presented in Table III. While the composite corners lack statistical significance, there is statistical confidence in that part of the composite consisting of the along-mean-wind and cross-mean-wind groups. Along these axes, general symmetries exist with strongest $w'T_v'$ being at the middle center of the composite. All fluxes within the composite are down-gradient. This finding is in agreement with those of Khalsa and Greenhut (1985) for their lowest levels.

The planview CD buoyancy flux composite is presented in Table IV. Statistical significance in the $w'T_v'$ pattern is

similar to that of the CU. The along-mean-wind and cross-mean-wind group axes are more symmetric than in the CU while the diagonal-to-the-mean-wind group axis is even more

TABLE III

CU buoyancy flux composite and corresponding standard deviations.

$w'T_v'$ ($ms^{-1}{}^oC$) (std. dev.)	Left	Center	Right
Downwind	0.024 (0.021)	0.010 (0.002)	0.024 (0.021)
Middle	0.010 (0.002)	0.018	0.011 (0.002)
Upwind	0.006 (0.008)	0.014 (0.002)	0.006 (0.008)

asymmetric in the along-mean-wind direction than in the CU.

The pattern of the CD $w'T_v'$ magnitude is similar to that of the CU. However, not all fluxes are positive. Fluxes found within the upwind left and right bins, although not statistically significant, are counter-gradient. In contrast and as will be seen in sub-section 3.3., all fluxes composing the CD absolute humidity composite CU of this study are down-

gradient. Keeping in mind the lack of statistical confidence, the upwind left and right bins of $w'T_v'$ for the CD composite, then, depart from findings of Khalsa and Greenhut (1985) that warm dry downdrafts have negative buoyancy flux only at levels

TABLE IV

CD buoyancy flux composite and corresponding standard deviations.

$w'T_v'$ ($ms^{-1}{}^oC$) (std. dev.)	Left	Center	Right
Downwind	0.009 (0.005)	0.005 (0.001)	0.009 (0.005)
Middle	0.004 (0.001)	0.006	0.004 (0.001)
Upwind	-0.002 (0.009)	0.004 (0.001)	-0.002 (0.009)

higher than the surface layer. Similar to what is suggested in Khalsa and Greenhut (1985) for some of their anomalous patterns, the counter-gradient $w'T_v'$ of this study may result from entrainment of buoyant CU air into the upwind side of the CD. The positive buoyancy flux portion of the CD $w'T_v'$ composite of this study compares well with findings in the

lowest levels of Khalsa and Greenhut (1985).

Of final note: a surface layer counter-gradient heat flux is found in the upwind region of the ensemble downdraft of Wilczak's (1984) vertical cross section. Thus, the finding of Wilczak (1984) compares well with the current study.

3.3. ABSOLUTE HUMIDITY FLUX

The planview CU absolute humidity flux composite is presented in Table V. Statistical confidence in w'r' exists

TABLE V

CU absolute humidity flux composite and corresponding standard deviations.

$w'r'(gs^{-1}m^{-2})$ (std. dev.)	Left	Center	Right
Downwind	0.045 (0.003)	0.041 (0.005)	0.045 (0.003)
Middle	0.039 (0.005)	0.068	0.041 (0.008)
Upwind	0.049 (0.003)	0.053 (0.010)	0.049 (0.003)

for all bins of the composite. As is expected by parcel displacement theory for a CMASL, flux in all bins of the composite is down-gradient. This property is also found in the majority of updrafts and downdrafts of Khalsa and Greenhut (1985). Composite patterns of w'r' resemble, for the most part, those of w'w'. The largest flux magnitude is found in the middle center bin. Fluxes along the upwind side of the draft is slightly larger than those on the downwind side. There is, however, symmetry along the cross-mean-wind group axis.

The CD w'r' composite is presented in Table VI. As with

TABLE VI

CD absolute humidity flux composite and corresponding standard deviations.

$w'r'(gs^{-1}m^{-2})$ (std. dev.)	Left	Center	Right
Downwind	0.025 (0.003)	0.025 (0.003)	0.025 (0.003)
Middle	0.023 (0.004)	0.034	0.022 (0.003)
Upwind	0.020 (0.002)	0.021 (0.002)	0.020 (0.002)

the CU, there is statistical confidence in the entire composite and the absolute humidity flux is down-gradient throughout the composite, with a maximum at the center. There are, however, some differences from the CU w'r' composite. As is expected from parcel displacement theory and the relative magnitudes of flux in the w'w' draft composites, a weaker absolute humidity flux composite is observed for the CD. Also, the downwind side of the CD composite contains slightly stronger flux than that of the upwind side but as in the CU composite, symmetry exists along the cross-mean-wind group axis.

3.4 MOMENTUM FLUX

There is statistical confidence for all bins of the CU planview along-mean-wind momentum flux composite, presented in Table VII. The flux contained in all bins are down-gradient, given the usual sign of the surface layer wind shear. This same property is seen in moist updrafts by Khalsa and Greenhut (1985). Wilczak (1984), however, shows a region of counter-gradient momentum flux just inside the trailing edge of his ensemble updraft vertical cross section. The largest flux magnitude in the CU composite is found in the middle center bin. Less significant asymmetries exist. For example, w'u' is stronger along the downwind side of the composite than along the upwind side. Weakest flux is found in the middle

left and right bins.

The CD planview flux composite of w'u' is presented in Table VIII. Statistical confidence exists in all data with

TABLE VII

CU along-mean-wind momentum flux composite and corresponding standard deviations.

$w'u'(m^2s^{-2})$ (std. dev.)	Left	Center	Right
Downwind	-0.133 (0.008)	-0.145 (0.041)	-0.133 (0.008)
Middle	-0.107 (0.016)	-0.219	-0.099 (0.018)
Upwind	-0.122 (0.023)	-0.123 (0.037)	-0.122 (0.023)

the exception of the upwind center bin, where the standard deviation approaches the magnitude of the flux. As with the CU, and as seen in Khalsa and Greenhut (1985), w'u' is down-gradient throughout the composite. As discussed below, this finding differs from that of Wilczak (1984) for his ensemble downdraft vertical cross section of w'u'. The region of strongest flux within the CD composite is found on the

downwind side, while weakest flux is on the upwind side. The largest magnitude of w'u' is seen in the downwind center bin while the smallest is in the upwind center bin. Cross-mean-wind group axis symmetry is seen.

As stated above, Wilczak (1984), using finer observational resolution than was possible in this study, shows a region of counter-gradient momentum flux just inside

TABLE VIII

CD along-mean-wind momentum flux composite and corresponding standard deviations.

$w'u'(m^2s^{-2})$ (std. dev.)	Left	Center	Right
Downwind	-0.077 (0.014)	-0.092 (0.027)	-0.077 (0.014)
Middle	-0.065 (0.015)	-0.084	-0.063 (0.016)
Upwind	-0.043 (0.008)	-0.028 (0.022)	-0.043 (0.008)

the trailing edge of his ensemble updrafts and downdrafts. Given the differences in horizontal resolution, it is possible that the along-mean-wind asymmetries in both studies are

related.

4. Summary

The coupling of the atmosphere to the ocean surface is accomplished predominately through fluxes induced by drafts within the marine atmospheric surface layer. Planview composite draft eddy correlation flux patterns of vertical velocity, buoyancy, absolute humidity, and the along-mean-wind component of momentum, within the convective marine atmospheric surface layer, are derived in this study. High resolution turbulence data are obtained from 20 NCAR Electra 50 m mean sea level flight legs from Project FIRE. Data processing results in a demeaned, detrended, despiked, high-pass filtered perturbation dataset.

A conditional sampling technique is used to isolate updrafts and downdrafts of interest from the environment. The technique uses horizontal scale and magnitude thresholds based on w′ event criteria. The w′ dataset is band-pass filtered to eliminate the inertial subrange contribution (0.1 Z_i cutoff wavelength) and the mesoscale contribution (1.5 Z_i cutoff wavelength). The minimum draft width is 50 m while 0.1 m/s is the w′ magnitude threshold. This technique results in the isolation of 2839 updrafts, averaging 98 m in width, and 3062 downdrafts, averaging 107 m in width.

After the identification of drafts of interest, eddy correlation fluxes are calculated for those portions of the processed dataset where drafts of interest are located. Mean

wind positioning within drafts, draft symmetry, and mean draft intensity are used to implement a series of averaging calculations, grouping techniques, and scaling operations.

The result of the above data manipulation is a planview composite updraft and downdraft for each flux discussed. The composites are composed of flux data located in horizontal three bin by three bin arrays. Each bin represents a mean-wind-relative sector of a composite draft: upwind, middle, or downwind by left, center, or right. Along-mean-wind group axes extend through the center of composite drafts while cross-mean-wind group axes extend through the middle of composite drafts.

Statistical confidence exists in the two vertical velocity flux composites. The strongest flux region of the updraft composite is located along the along-mean-wind group axis, with the largest magnitude flux found at the center of the draft. While the largest magnitude of $w'w'$ within the downdraft composite is also found at the center of the draft, the overall composite is weaker and more uniform than that of the updraft. In the buoyancy flux composites, only data in bins along the along-mean-wind and cross-mean-wind group axes are statistically significant. Along these axes, symmetries exist and the fluxes are down-gradient. Statistical confidence exists throughout both absolute humidity flux composites. As is expected by parcel displacement theory, all fluxes are down-gradient. The largest magnitudes of flux are

found in the middle center bins, and both composites show cross-mean-wind group axis symmetry. The updraft and downdraft along-mean-wind component of momentum flux composites are statistically significant throughout, with the exception of the upwind center bin of the downdraft composite. All fluxes of both composites are down-gradient. The largest flux magnitude for the updraft is in the middle center bin while that of the downdraft is located in the downwind center bin. Along-mean-wind asymmetry exists within both composites with downwind bins having greater magnitudes of flux than upwind bins.

It is hoped that this study provides new useful insight into the planview flux structure of CMASL updrafts and downdrafts. The degree of spatial resolution in these results, as well as the techniques presented in this study, could be of use in verification of nonlinear convective boundary layer models such as that presented in Haack and Shirer (1992). These results are also appropriate for the input of forcing in time dependent two-dimensional ocean wave models of cats paw-type features.

Of course much room exists for improvement upon and expansion beyond this study. This study should be used as a stepping stone for such research initiatives.

Acknowledgements

We would like to thank H. N. Shirer, S. J. S. Khalsa and K. A. Moyer for valuable discussions and suggestions. Also we would like to thank the anonymous reviewer for the very useful comments. The research reported in this work was funded by the Office of Naval Research under Grant N00014-90-J-4012.

References

Albrecht, B. A., Randall, D. A., and Nicholls, S.: 1988, 'Observations of Marine Stratocumulus Clouds During FIRE', *Bull. Amer. Meteorol. Soc.* **69**, 618-626.

Dorman, C. E. and Mollo-Christensen, E.: 1973, 'Observation of the Structure on Moving Gust Patterns Over a Water Surface ("Cat's Paws")', *J. Phys. Ocean.* **3**, 120-132.

Gaynor, J. E., and Mandics, P. A.: 1978, 'Analysis of the Tropical Marine Boundary Layer During GATE Using Acoustic Sounder Data', *Mon. Wea. Rev.* **106**, 223-232.

Geernaert, G. L., and Hansen, F.: 1992, 'Low Frequency Variability of the Wind Stress Vector in the Surface Layer Over the Sea', *Preprints Tenth Symp. on Turbulence and Diffusion*, Portland, Amer. Meteor. Soc.

Greenhut, G. K., and Khalsa, S. J. S.: 1982, 'Updraft and Downdraft Events in the Atmospheric Boundary Layer Over the Equatorial Pacific Ocean', *J. Atmos. Sci.* **39**, 1803-1818.

Haack, T., and Shirer, H. N.: 1992, 'Mixed Convective-Dynamic Vortices and Their Effects on Initial Wind and Temperature Profiles', *J. Atmos. Sci.* **49**, 1181-1201.

Khalsa, S. J. S., and Greenhut, G. K.: 1985, 'Conditional Sampling of Updrafts and Downdrafts in the Marine Atmospheric Boundary Layer', *J. Atmos. Sci.* **42**, 2550-2562.

Kloesel, K. A., Albrecht, B. A., and Wylie, D. P.: 1988, 'FIRE Marine Stratocumulus Observations-Summary of Operations and Synoptic Conditions', Penn State University, Department of Meteorology, FIRE Technical Report No. 1.

Lenschow, D. H. and Stephens, P. L.: 1980, 'The Role of Thermals in the Convective Boundary Layer', *Boundary-Layer Meteorol.* **19**, 509-532.

Liu, W.T., Katsaros, K.B., and Businger, J.A.: 1979, 'Bulk Parameterization of the Air-Sea Exchanges of Heat and Water Vapor Including the Molecular Constraints at the Interface', *J. Atmos. Sci.* **36**, 1722-1735.

Moyer, K. A. and Young, G. S.: 1991, 'Observations of Vertical Velocity Skewness Within the Marine Stratocumulus-Topped Boundary Layer', *J. Atmos. Sci.* **48**, 403-410.

Nucciarone, J. J. and Young, G. S.: 1991, 'Aircraft Measurements of Turbulence Spectra in the Marine Stratocumulus-Topped Boundary Layer', *J. Atmos. Sci.* **48**, 2382-2392.

Schumann, U. and Moeng, C.-H.: 1991, 'Plume Fluxes in Clear and Cloudy Convective Boundary Layers', *J. Atmos. Sci.* **48**, 1746-1757.

Stull, R. B.: 1988, *An Introduction to Boundary Layer Meteorology*, Kluwer Academic Publishers, Dordrecht.

Wilczak, J. M.: 1984, 'Large-Scale Eddies in the Unstably Stratified Atmospheric Surface Layer. Part I: Velocity and Temperature Structure', *J. Atmos. Sci.* **41**, 3537-3550.

Wilczak, J. M. and Tillman, J. E.: 1980, 'The Three-Dimensional Structure of Convection in the Atmospheric Surface Layer, *J. Atmos. Sci.* **37**, 2424-2443.

Woodcock, A. H.: 1940, 'Convection and Soaring Over the Open Sea', *J. Marine Res.* **3**, 248-253.

Woodcock, A. H.: 1975, 'Thermals Over the Sea and Gull Flight Behavior', *Boundary-Layer Meteorol.* **9**, 63-68.

Young, G. S.: 1987, 'Mixed Layer Spectra From Aircraft Measurements', *J. Atmos. Sci.* **44**, 1251-1256.

Young, G. S.: 1988, 'Turbulence Structure of the Convective Boundary Layer. Part II: Phoenix 78 Aircraft Observations of Thermals and Their Environment', *J. Atmos. Sci.* **45**, 727-735.

Reprinted from the preprint volume of the Tenth Symposium on Turbulence and Diffusion, 29 Sept. - 2 Oct. 1992, Portland, OR.
Published by the American Meteorological Society, Boston, MA

P1.6

AIR/SEA FLUX PATTERNS WITHIN CONVECTIVE STRUCTURES OF THE MARINE ATMOSPHERIC SURFACE LAYER

Todd D. Sikora and George S. Young

The Pennsylvania State University
University Park, Pennsylvania

1. INTRODUCTION

Air/sea fluxes of heat, moisture, and momentum are realized predominantly through sub-mesoscale convectively driven updrafts (CDUs) and downdrafts (CDDs), diameters of which are on the order of tens to thousands of meters (Lenschow and Stephens, 1980; Khalsa and Greenhut, 1985). Various analysis methods may be employed to study these drafts. One approach is to observe the effect of the drafts on other aspects of the atmosphere or ocean, such as cat's-paw wave packets or cumulus clouds. A more quantitative approach, taken in this study, involves sampling the turbulent fluctuations of temperature, moisture, and velocity within the drafts. Conditional sampling of observed or modeled turbulence fields has been proven to be effective in the quantitative analysis of convective draft structure and dynamics (Lenschow and Stephens, 1980; Wilczak and Tillman, 1980; Greenhut and Khalsa, 1982; Wilczak, 1984; Khalsa and Greenhut, 1985; Young, 1988; Schumann and Moeng, 1991).

While this previous work has resulted in detailed vertical profiles of properties of marine atmospheric boundary layer (MABL) updrafts and downdrafts, information on planview flux variability of these MABL CDUs and CDDs is lacking. Our study uses conditionally sampled and composited eddy correlated FIRE (First ISCCP (International Satellite Cloud Climatology Project) Regional Experiment) aircraft data to investigate the typical CDU and CDD planview flux patterns of vertical velocity (w'), buoyancy (t_v'), absolute humidity (r'), and along-mean-wind momentum (u') in the convective marine atmospheric surface layer (CMASL).

2. PROCEDURES

The use of NCAR Electra turbulence measurements from Project FIRE is advantageous for our analysis. During FIRE, the Electra collected high resolution turbulence data from a large number of drafts within the CMASL. While each draft was penetrated only once, penetrations of many different drafts were made from numerous angles relative to the mean wind. Data were obtained from 20 horizontal legs flown at 50 m MSL. Each leg was approximately 50 km (500 sec) in length. These legs were flown over a period of seven days in July, 1987 off the coast of California. The boundary layer depth (Z_i) averaged 920 m during these legs so the 50 m flight level was well within the surface layer. Ratios of the boundary layer depths to the Monin-Obukhov lengths ranged from -0.62 to -37.56, indicative of slightly to moderately unstable MABLs.

This study uses the same instrumentation reviewed by Nucciarone and Young (1991). Data preprocessing for mean and trend removal parallels that of Lenschow and Stephens (1980). Mesoscale phenomena are eliminated from the data series using the highpass filtering techniques of Young (1987, 1988) incorporating a 1.5 Z_i cutoff wavelength based on the spectra of Nucciarone and Young (1991). Coordinate transformations are performed on the resulting perturbation wind components yielding one in the direction of the mean wind, u', and another aligned with positive values 90° to the left of the mean wind (v'). The latter is both statistically and physically insignificant (ie. small in magnitude) when compared with the alongwind component and, therefore, its flux is not discussed.

Conditional sampling to distinguish updrafts and downdrafts uses event criteria based on w', following Greenhut and Khalsa (1982), and incorporates germane horizontal scale and magnitude thresholds, following Young (1988). Thus, for event identification, the w' series is bandpass filtered to eliminate the inertial subrange contribution (0.1 Z_i cutoff wavelength) and the mesoscale contribution (1.5 Z_i cutoff wavelength as mentioned above). The inertial subrange contribution is, in contrast, retained in the data series used for eddy correlation statistic computation. Given the average Z_i of this study, a minimum draft width of 50 m is chosen so that the shortest acceptable updraft/downdraft couplet corresponds with the 0.1 Z_i inertial subrange cutoff wavelength used in the bandpass filter. Inspection of the FIRE w' data series suggests that a w' threshold of $\pm$ 0.1 m/s eliminates disorganized areas of weak ascent or descent. 0.1 m/s is therefore used as the magnitude threshold in our study. Any data series segment not meeting the above criteria is not considered to be part of a significant convective draft and is rejected. This method yields 2839 CDUs averaging 98 m in width and 3062 CDDs averaging 107 m in width.

After the isolation of CDUs and CDDs from each leg, as discussed above, eddy correlation fluxes are calculated for each draft. In order to develop typical planview flux snapshots, the fluxes from all the drafts are composited together using a series of averaging calculations and grouping techniques. Each draft is first divided into three bins of equal length: the aircraft entry region of the draft, the middle of the draft, and the aircraft exit region of the draft. The average CDU and CDD flux patterns for each leg are then found by calculating the bin average eddy correlation statistics.

The resulting 40 leg average drafts from the 20 flight legs are then separated into three equal angular-width groups based on the path taken by the aircraft through the draft, relative to the mean wind. In polar coordinates aligned with the mean wind blowing towards 0°, these relative heading groups are: alongwind (330° to 30°), crosswind (60° to 120°), and diagonal to the wind (30° to 60°). To maintain relative-wind consistency, the entry and exit bins are swapped for headings opposite of those given above. Draft symmetry around the alongwind axis (Wilczak, 1984) justifies combining the data from all four sectors diagonal to the wind into the one given above. Our crosswind composites verify this symmetry. Corresponding bin averages for each heading group are composited, yielding a typical CDU flux pattern and a corresponding CDD flux pattern for each flux statistic. Because of the need to correct for mean draft intensity differences between flight legs, the perimeter bin fluxes are rescaled before compositing. This rescaling uses a correction coefficient based on the requirement for similarity in the middle bins, where all heading groups are assumed to overlap.

3. RESULTS

Planview draft flux composites of vertical velocity ($\overline{w'w'}$), buoyancy ($\overline{w't_v'}$), absolute humidity ($\overline{w'r'}$), and along-mean-wind momentum ($\overline{w'u'}$), are found in Tables 1 through 4. The tables labeled (A) contain CDU flux composites while tables labeled (B) contain CDD flux composites. Each table is a three by three

horizontal array of fluxes obtained from the bin averaging and grouping techniques described in the previous section. For all tables, the mean wind is directed towards the top of the page.

The planview CDU and CDD vertical velocity flux composites are shown in Tables 1A and 1B. Because all bin standard deviations are much smaller than the corresponding fluxes (less than 1/3 of these means), there is statistical confidence in the $\overline{w'w'}$ composites. Both flux composites are nearly symmetric across the axis of the mean wind. The strongest flux region in the CDU composite is found on the alongwind axis with the largest magnitude of flux being at the draft center. This shape compares well with that found at 50 m over land by Wilczak (1984). While the largest magnitude of $\overline{w'w'}$ in the CDD composite is also found in the center bin, the overall flux composite is more uniform than that of the CDU and is weaker, in agreement with findings of Greenhut and Khalsa (1982).

Table 1A. CDU vertical velocity flux composite.

$\overline{w'w'}$ (m^2s^{-2})	Left	Center	Right
Downwind	0.227	0.244	0.227
Middle	0.217	0.341	0.225
Upwind	0.238	0.266	0.238

Table 1B. CDD vertical velocity flux composite.

$\overline{w'w'}$ (m^2s^{-2})	Left	Center	Right
Downwind	0.160	0.161	0.160
Middle	0.171	0.204	0.173
Upwind	0.162	0.166	0.162

The buoyancy flux of the current study approximates, to a large extent, the heat flux. The planview CDU and CDD $\overline{w't_v'}$ composites are shown in Tables 2A and 2B. There is statistical confidence in those parts of the composites made up of the along wind and crosswind groups but not in the diagonal elements (array corners). Alongwind and crosswind symmetries exist for both the CDU and CDD composite. All statistically significant fluxes within the composites are down-gradient, in agreement with the lowest levels of Khalsa and Greenhut (1985).

Table 2A. CDU buoyancy flux composite.

$\overline{w't_v'}$ ($ms^{-1}{}^{o}C$)	Left	Center	Right
Downwind	0.024	0.010	0.024
Middle	0.010	0.018	0.011
Upwind	0.006	0.014	0.006

Table 2B. CDD buoyancy flux composite.

$\overline{w't_v'}$ ($ms^{-1}{}^{o}C$)	Left	Center	Right
Downwind	0.009	0.005	0.009
Middle	0.004	0.006	0.004
Upwind	-0.002	0.004	-0.002

The planview CDU and CDD absolute humidity flux composites are shown in Tables 3A and 3B. Statistical confidence of $\overline{w'r'}$ exists in all bins of both composites. As is expected by parcel displacement theory, the flux composites are down-gradient, as is found in the majority of updrafts and downdrafts of Khalsa and Greenhut (1985). Similar to the $\overline{w'w'}$ composites, the largest flux magnitude is found in the middle bin. Flux along the upwind side of the CDU composite and downwind side of CDD composite is slightly larger than that of the opposite side of each respective composite. There is, however, good crosswind symmetry in both.

Table 3A. CDU absolute humidity flux composite.

$\overline{w'r'}$ ($gs^{-1}m^{-2}$)	Left	Center	Right
Downwind	0.045	0.041	0.045
Middle	0.039	0.068	0.041
Upwind	0.049	0.053	0.049

Table 3B. CDD absolute humidity flux composite.

$\overline{w'r'}$ ($gs^{-1}m^{-2}$)	Left	Center	Right
Downwind	0.025	0.025	0.025
Middle	0.023	0.034	0.022
Upwind	0.020	0.021	0.020

The CDU and CDD planview $\overline{w'u'}$ composites are shown in Tables 4A and 4B. There is statistical confidence in the fluxes of all bins except that of the upwind center bin in the CDD composite. All fluxes of both composites are down-gradient, given the usual surface layer vertical wind shear. This same property is seen in similar drafts of Khalsa and Greenhut (1985). The largest CDU flux magnitude is again at the center of the draft while the CDD flux magnitude maximum is located at the downwind center. The CDU flux magnitude does, however, show some tendency towards this form of asymmetry with the downwind bins having greater magnitudes than the upwind bins. Wilczak (1984), using finer horizontal resolution, shows a region of counter-gradient momentum flux just inside the upwind edge of his ensemble updrafts and downdrafts. Given the differences in horizontal resolution, it is possible that the alongwind asymmetries in both studies are related.

Table 4A. CDU along-mean-wind momentum flux composite.

$\overline{w'u'}$ (m^2s^{-2})	Left	Center	Right
Downwind	-0.133	-0.145	-0.133
Middle	-0.107	-0.219	-0.099
Upwind	-0.122	-0.123	-0.122

Table 4B. CDD along-mean-wind momentum flux composite.

$\overline{w'u'}$ (m^2s^{-2})	Left	Center	Right
Downwind	-0.077	-0.092	-0.077
Middle	-0.065	-0.084	-0.063
Upwind	-0.043	-0.028	-0.043

4. ACKNOWLEDGEMENTS

We wish to thank Drs. Khalsa and Shirer for valuable discussions. Funding for this research has been through the Office of Naval Research under grants N00014-90-J-4012 and N00014-91-J-1992.

5. REFERENCES

Greenhut, G. K., and S. J. S. Khalsa, 1982: Updraft and downdraft events in the atmospheric boundary layer over the equatorial Pacific Ocean. *J. Atmos. Sci.*, 39, 1803-1818.

Khalsa, S. J. S., and G. K. Greenhut, 1985: Conditional sampling of updrafts and downdrafts in the marine atmospheric boundary layer. *J. Atmos. Sci.*, 42, 2550-2562.

Lenschow, D. H., and P. L. Stephens, 1980: The role of thermals in the convective boundary layer. *Bound-Layer Meteor.*, 19, 509-532.

Nucciarone, J. J., and G. S. Young, 1991: Aircraft measurements of turbulence spectra in the marine stratocumulus-topped boundary layer. *J. Atmos. Sci.*, 48, 2382-2392.

Schumann, U. and C.-H. Moeng, 1991: Plume fluxes in clear and cloudy convective boundary layers. *J. Atmos. Sci.*, 48, 1746-1757.

Wilczak, J. M., 1984: Large-scale eddies in the unstably stratified atmospheric surface layer. Part I: Velocity and temperature structure. *J. Atmos. Sci.*, 41, 3537-3550.

Wilczak, J. M., and J. E. Tillman, 1980: The three-dimensional structure of convection in the atmospheric surface layer. *J. Atmos. Sci.*, 37, 2424-2443.

Young, G. S., 1987: Mixed layer spectra from aircraft measurements. *J. Atmos. Sci.*, 44, 1251-1256.

Young, G. S., 1988: Turbulence structure of the convective boundary layer. Part II: Phoenix 78 aircraft observations of thermals and their environment. *J. Atmos. Sci.*, 45, 727-735.

OFFICE OF NAVAL RESEARCH
PUBLICATIONS/PATENTS/PRESENTATIONS/HONORS REPORT
1 Oct 91 through 30 Sep 92

R&T Number: 4215021---03

Contract/Grant Number: N00014-90-J-4012

Contract/Grant Title: SAR-Related Stress Variability in the Marine Atmospheric Boundary Layer (MABL)

Principal Investigator: H.N. Shirer and G.S. Young

Mailing Address: 503 Walker Building, Department of Meteorology, Penn State University, University Park, PA 16802

Phone Number: (with Area Code) 814-863-1992 (HNS); 814-863-4228 (GSY)

E-Mail Address: HNS@PSUVM.PSU.EDU; G.Young/Omnet

a. Number of Papers Submitted to Refereed Journal but not yet published: 0

b. Number of Papers Published in Refereed Journals: 1 (list attached)

c. Number of Books or Chapters Submitted but not yet Published: 0

d. Number of Books or Chapters Published: 0 (list attached)

e. Number of Printed Technical Reports & Non-Refereed Papers: 3 (list attached)

f. Number of Patents Filed: 0

g. Number of Patents Granted: 0 (list attached)

h. Number of Invited Presentations at Workshops or Prof. Society Meetings: 6

i. Number of Presentations at Workshops or Prof. Society Meetings: 2

j. Honors/Awards/Prizes for Contract/Grant Employees: NONE
(list attached, this might include Scientific Soc. Awards/ Offices, Promotions/Faculty Awards/Offices, etc.)

k. Total number of Graduate Students and Post-Docs Supported at least 25% this year on this contract/grant:

Grad Students 4 and Post-Docs 1 including 0
Grad Student Female 0 and Post-Docs Female 0
Grad Student Minority 1 and Post-Doc Minority 0

Minorities include Blacks, Aleuts, AmIndians, Hispanics, etc.
NB: Asians are not considered an under-represented or minority group in science and engineering.

Enclosure (3)

Refereed Papers

Sikora, T.D. and G.S. Young, 1993: Observations of planview flux patterns within convective structures of the marine atmospheric surface layer, *Boundary Layer Meteorology*, **35**, in press.

Non-Refereed Papers

Hare, J.E, 1992: Shipboard eddy-covariance measurements of the turbulent fluxes of heat, moisture, and momentum. MS Thesis, Penn State University, 207 pp.

Sikora, T.D., 1992: Air/sea flux patterns within convective structures of the marine atmospheric surface layer, MS Thesis, Penn State University, 28 pp.

Sikora, T.D and G.S. Young, 1992, Air/sea flux patterns within convective structures of the marine atmospheric surface layer, Preprints, *Tenth Symposium on Turbulence and Diffusion*, Sept. 29-Oct. 2, 1992, Portland, OR, American Meteorological Society, 25-27.

Planview of Composite Downdraft Horizontal Wind

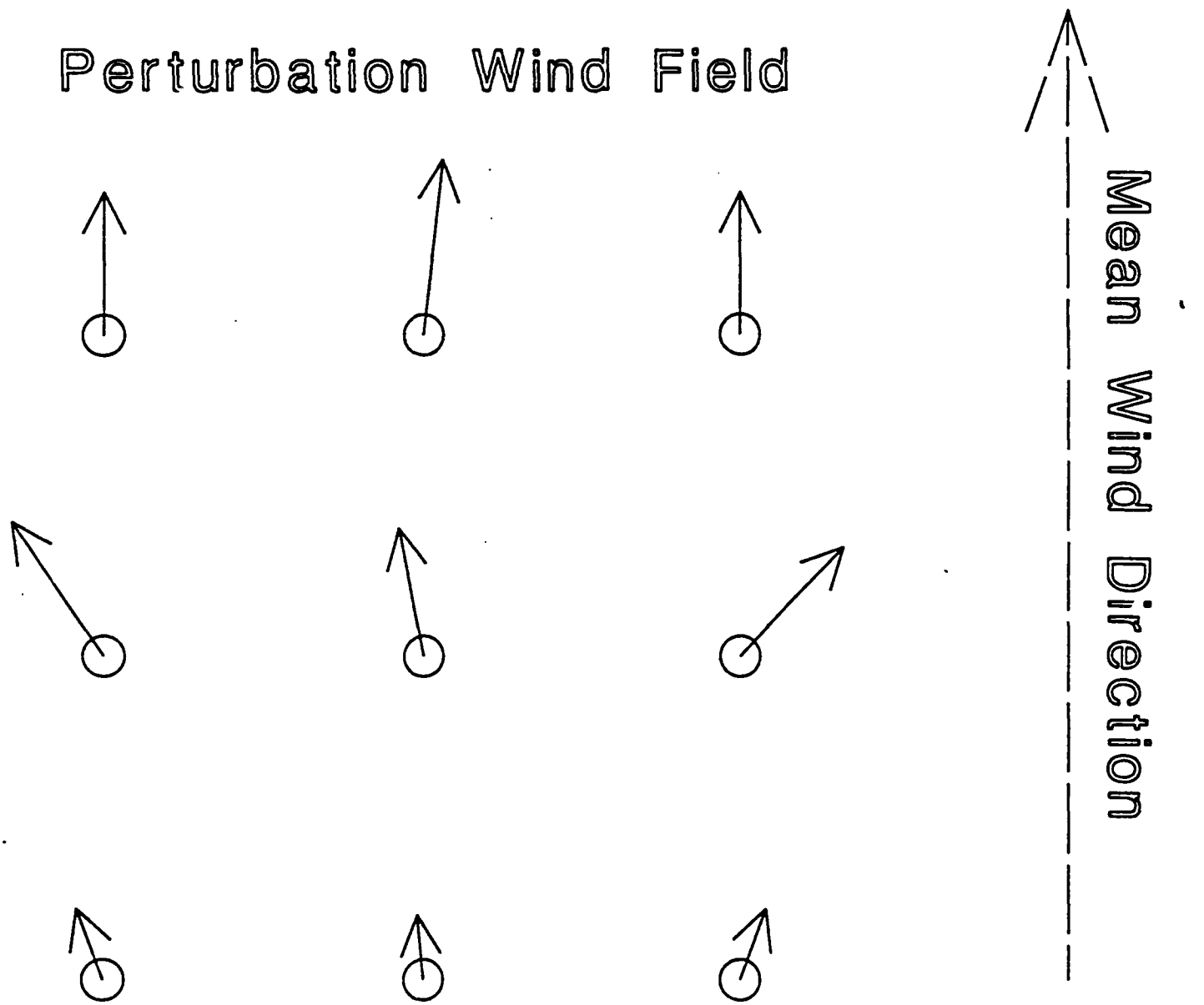

Planview of Convective Updraft/Downdraft Field

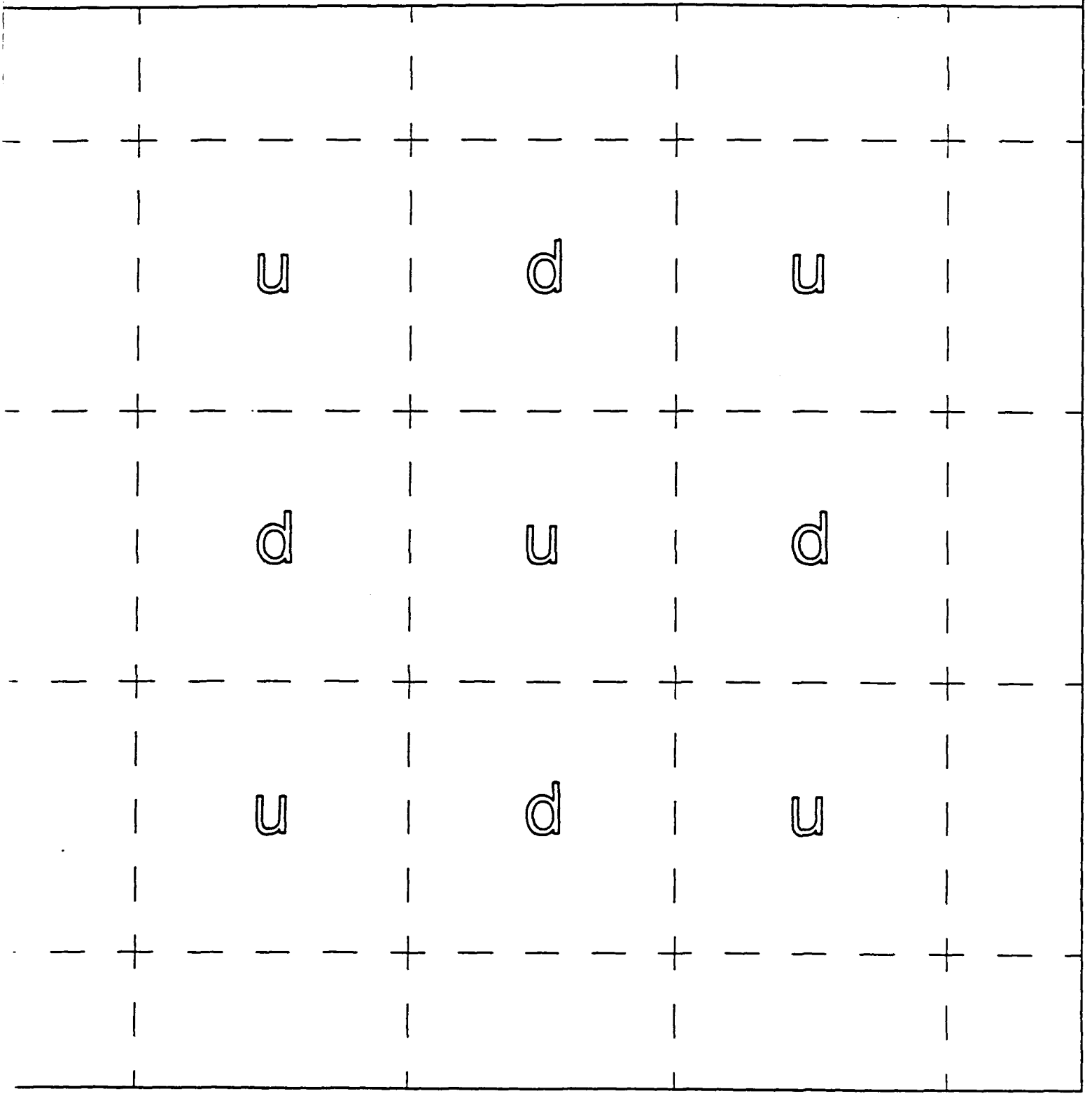

Planview of Composite Updraft Horizontal Wind